EG UK Theory and Practice of Computer Graphics (2008)
Ik Soo Lim, Wen Tang (Editors)

Segmenting the External Surface of a Human Skull in MR Data

M. Salas and S. Maddock

Department of Computer Science, University of Sheffield, UK
Email: {M.Salas | S.Maddock}@dcs.shef.ac.uk

Abstract

A method is presented to extract the outline of the skull region in coronal Magnetic Resonance (MR) images from the Visible Human Project. The starting point is the formulation of a Gradient Vector Flow (GVF) snake extended to include statistical shape information. This method exploits the diffusion process used by the GVF snake and improves its capacity to deal with occlusion problems by adding a shape term to the traditional scheme. The results of the segmentation of the MR data are compared with the results of the segmentation of CT scans of the same individual. For the MR data, the addition of a shape term improves on the results obtained by using a GVF snake alone.

Categories and Subject Descriptors (according to ACM CCS): I.4.6 [Image Processing and Computer Vision]: Edge and feature detection I.4.7 [Image Processing and Computer Vision]: Size and shape I.3.3 [Computer Graphics]: Boundary representations

1. Introduction

The process of skull segmentation in medical images is an important step toward a complete segmentation of tissue in the human head [RBH*99], but is difficult to automate using current techniques. Our work aims to address this and thus promote study of the relationship between the skull and the face. In particular we are interested in the area of forensic facial reconstruction [KHS03, VVMN00, Wil04]. Forensic facial reconstructions are usually carried out by using tables of tissue depth measurements at discrete landmark points on the human face [Wil04]. By using MRI data to extract the complete skull-skin relationship, our aim is to improve upon the use of such discrete data sets, and thus produce better computer-based reconstructions.

In our approach, we extract the skull surface by bi-dimensionally segmenting a set of images of an MR volume. The extracted contours are then assembled to create a 3D skull model. At each slice, the skull region is segmented as a single contour or as a combination of several partial skull contours. The extracted contours are then assembled to create a 3D skull model.The segmentation process is made up of two components. The first component is an active contour [KWT88, IT98] directed by image features which 'blindly' tries to enclose skull areas. The second component is a shape term [CTWS02] which adds statistical knowledge of the likely shape to find. The two components are combined to make an active contour evolve towards a minimum within the static potential field calculated from the

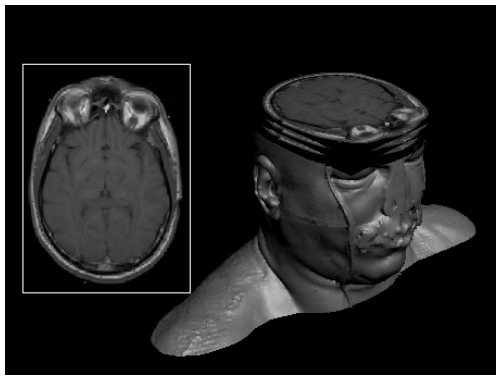

Figure 1: *The magnetic resonance male dataset from the VHP project [Ack98, SASW96]. Left: a typical MR scan image. Right: the structure of the volume.*

gradient information in an image. To test our approach, we use the Magnetic Resonance (MR) 3D dataset of the male head from the Visible Human Project [Ack98, SASW96]. Figure 1 illustrates the multiple slice structure of this dataset. A Computer Tomography (CT) volume of the same person is also available. Figure 2 shows an example of two modalities for the eye socket region, which is one of the most complicated regions for skull segmentation in MR images due to the high variability of pixel intensities of the bone components [HHP*97]). To assess the performance of our proposed algorithm, the results of the MR segmentation will be compared with the results of segmenting the same bone area in a CT image, which is relatively straightforward to segment.

In the field of medical imaging, there are several approaches available for dealing with segmentation issues. Approaches such as region growing [HHP*97], level-sets [HF04] and deformable models [KWT88, IT98] have been successfully applied to segmentation of specific tissue types in MRI images such as white matter, grey matter and cerebrospinal fluid. However, MRI skull segmentation has received little research in the last years [SHJ*07]. The complex topology of the skull, the high pixel intensity variations present in some skull areas, and the existence of thin regions of skull, which are difficult to detect with current MRI sampling resolutions, are the principal issues that complicate this task.

One of most important problems to solve to achieve a complete MRI tissue classification is the partial volume effect, which is the situation where one voxel of the volume may contain multiple tissue types. Most of the techniques used for MRI tissue classification work under the assumption that the tissue types of each voxel can be separated by means of the statistical properties of their intensities. For example, in the work of Laidlaw et. al. [LFB98] a Bayesian partial volume classification is proposed with a number of restrictions such as: discrete materials, sampling theorem satisfied and linear mixtures between the tissues (all of them difficult to guarantee in the case of the skull). Vandermeulen et. al. [LMVS03] also propose a similar approach for dealing with partial volume problems. Similarly, this work offers good results for brain tissues present in MRI but is not directly applicable to the skull.

Some attempts have been made to apply the above techniques to the problem of skull segmentation in MRI images. Dogdas et. al. [DSL02] propose a method in which the segmentation of the skull is done by using mathematical morphology operations in the spatial domain of the image. This work is a good example for illustrating that even having classified most of the tissues in a human head that are not bone, detecting the skull is still a problem. The work of Rifai et. al. [RBH*99] is one of the first attempts to include shape information in the skull segmentation, combining region growing and level-set techniques. Heinoen et. al. [HHP*97] propose some statistical models for tissue classification applied to the problem of detecting bone pixels and using thresholding and region growing algorithms. In [SHJ*07] a registration method is employed in which a set of skull models generated from CT segmentations is used for registering new data in MRI modalities. There is room for improvement in the results produced by these methods.

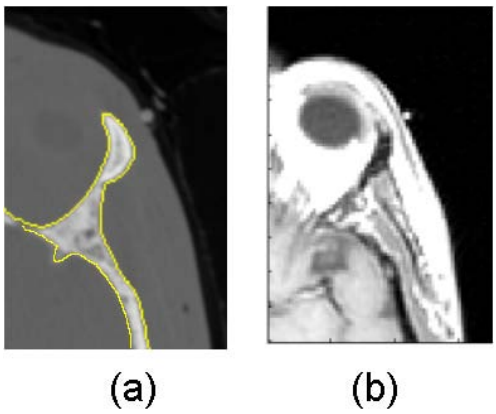

Figure 2: *A portion of a slice of a human head (from the VHP dataset) showing the same anatomical region, approximately at the level of the right eye with a view from above the head. (a) The CT scan version and (b) the MR version.*

In the field of deformable models, several approaches have been proposed to combine image features with shape information. For instance, Abram et. al. [AS99] include a statistical form of a shape in an active contour, which is modeled with a vector representation based on the centroid and orientation of a shape. Gunn [GN94] uses a dual active contour to define a region of convergence between an external and an internal active contour. Simple objects can be segmented with this combination under high quantities of noise. Fang et. al. [FC06] include the shape in a geodesic active contour in the form of PCAs of previously trained shapes. Cremers et. al. [CTWS02] propose a diffusion snake with the inclusion of a shape term and a dynamic potential field, which has to be calculated at each iteration of the snake evolution. Tejos et. al. [THCB06] have tested a diffusion active contour proposed by [CTWS02] to segment articular cartilage in MRI images.

The originality of our approach is the use of a deformable model using a static potential force defined as a gradient vectorial flow (GVF) in all the image domain. This combination is presented as an alternative to tackle some of the main problems in skull detection in MR images. We will demonstrate that this works where other techniques based on gradient (e.g. [XP97]) have difficulties. The proposed integration can offer the following advantages over other methods:

- The static potential can be calculated just once at the beginning of the process in contrast to other techniques that

use a dynamic approach (e.g. [PTT02]). This computation can also be parallelized.

- Gradient information can be exploited in regions where the contour is clearly defined by the gradient profile and shape information is used to contribute in areas where it is not possible to establish a clear border (e.g. in regions where the MR values fail to distinguish between skull and air).
- The gradient vector flow potential increases the range of capture (which is the region of influence of an object's edge on the active contour) and allows the evolution of the active contour through concave regions (in which two edges of the object contour are relatively near to each other and can counteract the contour evolution process), which is a problem with other gradient based approaches.

The rest of this document is organized as follows. Section 2 introduces active contour terminology, and the gradient vector flow (GVF) snake and its potential field. Section 3 describes the inclusion of statistical shape knowledge to the active contour formulation. Section 4 presents the experimental results and, finally, section 5 states the conclusions.

2. Gradient vector flow active contours

A traditional formulation for an active contour, or snake [CKS97, TWK88, KWT88, IT98], is a curve $x(s) = [x(s), y(s)]$, $s \in [0,1]$ that moves through the spatial domain Ω of an image in order to minimize: :

$$E_t = \int_0^1 (\frac{1}{2}(\alpha \left|x'(s)\right|^2 + \beta \left|x''(s)\right|^2 + E_{ext}(x(s)))ds \quad (1)$$

where $x'(s)$ and $x''(s)$ stand for the first and second derivative of the curve x with respect to s, and α and β are weighting parameters that control the active contour tension and rigidity [KWT88]. The external energy E_{ext} is obtained from the image and reaches its lower values at interest features such as boundaries.

Gradient vector flow (GVF) active contours are curves under the influence of a potential force called gradient vector flow [XP97]. The gradient vector flow is an external force computed as a diffusion of the gradient vectors of the image. This force is used to attract the snake towards the edges in the image. The evolution of a GVF snake can be formulated by solving equation (1) by minimizing the following Euler equation:

$$\alpha x''(s) + \beta x''''(s) - \nabla E_{ext} = 0 \quad (2)$$

To find a solution to equation (2) the snake is made dynamic by treating x as a function of time t as well as the spline parameter s. i.e. $x(s,t)$. Then a partial derivative of x with respect to t can be formulated as:

$$x_t(s,t) = \alpha x''(s,t) + \beta x''''(s,t) - \nabla E_{ext} \quad (3)$$

When the solution $x(s,t)$ stabilizes, the term $x_t(s,t)$ gradually disappears and we achieve a solution for equation (2). The GVF active contour used in this work uses the following potential force influencing the curve evolution:

$$\nabla E_{ext}(x,y) = -|\nabla I(x,y)|^2 \quad (4)$$

where $I(x,y)$ is the image intensity of pixel (x,y). The vector field $\mathbf{v}(x,y) = (u(x,y), v(x,y))$ associated with this potential force is obtained by minimizing the energy functional:

$$\varepsilon = \int \mu(u_x^2 + u_y^2 + v_x^2 + v_y^2) + |\nabla f|^2 |\mathbf{v} - \nabla f|^2 \, dxdy \quad (5)$$

where μ is a regularization parameter controlling the compromise between the first and second terms of the integral, and $f(x,y) = -E_{ext}(x,y)$ is an edgemap defined in the domain of the image. This functional has the effect of keeping $\mathbf{v}$ nearly equal to the gradient of the edge maps when ∇f is the most important component and varying in a smooth way in regular regions. Expressing the components of this vector field in terms of the time parameter t gives:

$$\begin{aligned} u_t(x,y,t) &= \mu\nabla^2 u(x,y,t) - (u(x,y,t) - f_x(x,y)) \\ &\quad \cdot(f_x(x,y)^2 + f_y(x,y)^2) \quad (6) \\ v_t(x,y,t) &= \mu\nabla^2 v(x,y,t) - (v(x,y,t) - f_y(x,y)) \\ &\quad \cdot(f_x(x,y)^2 + f_y(x,y)^2) \quad (7) \end{aligned}$$

A stable finite difference implementation for solving the steady-state of these equations is given in detail in [XP96]. The calculated field $\mathbf{v}$, after the minimization process, replaces the potential force ∇E_{ext} in equation (3). Figure 3(a) shows a CT image of an area around the right eye socket and in 3(b) its potential forces derived from the edges of the object (image features). Figure 4 shows the GVF of an MRI thresholded version of the same area shown in figure 3. Note that the skull region is partially defined and it will not be possible to segment if additional shape information is not included.

3. Including shape knowledge in the segmentation process

The shape term we use in this work is an adaptation of the one proposed by Cremers et al. [CTWS02]. For a contour $C = x(s)$ we consider the following extended energy :

$$E = E_t + \gamma E_c(C) \quad (8)$$

where the term E_t is the energy contribution of a GVF active contour, E_c benefits contours with similar shapes to the one acquired in a shape training process, and γ is a factor to regulate the amount of influence of the shape term.

In general terms, the training process consists of collecting a set of similar shaped objects. We adopt the concept of shape defined by Dryden [DM98], who defines the shape of an object as all the geometric features of the object that are unchanged when it is translated, rescaled and rotated in

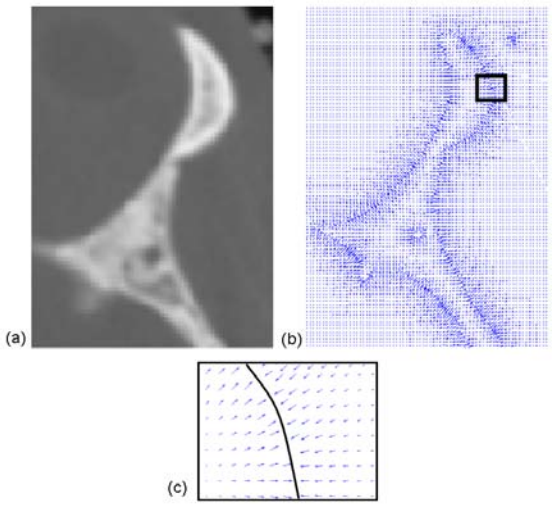

Figure 3: *A portion of the skull around the right eye socket (area presented in figure 2(a)). (a) Original gray level CT image. (b) GVF field of the image and the rectangular marked area enlarged (c). The black line in (c) represents a portion of the object boundary and the blue arrows the direction of the GVF potential forces.*

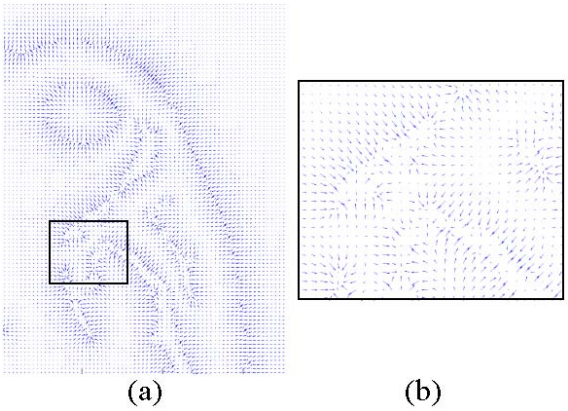

Figure 4: *The GVF of the MRI image presented in figure 2(b). (b)Detail of the GVF at the rectangular marked area enlarged.*

an arbitrary coordinate system. In this work, the set of geometric features corresponds to a set of points placed along the object contour. The labelling of the control points can be done manually or automatically and the main objective is to create a reference set of control points to model the statistical shape variation.

The effect of combining E_t and E_c is twofold. First, it augments the capture range of potential field forces (which leads to less sensitivity to initialization). Second, it improves the capacity of the snake to deal with occlusion problems by adding knowledge of the shape of the object to segment.

The following subsections describe the derivation of the Ec term of equation (8) which accounts for pre-established shape information.

3.1. Incorporating statistical shape information

In our work, the active contour C is represented with a quadratic B-spline curve:

$$C : [0,1] \rightarrow \Omega, \;\; C(s) = \sum_{i=1}^{n} p_i B_i(s) \tag{9}$$

where s is the parameter of the spline, p_i is the set of control points, and $B_i(s)$ are the quadratic periodic B-spline basis functions [Far97, BI98]. A 2D object shape z is represented by a set of n pairs of control points defining the curve. The shape z can be referred to as a unidimensional vector with the following structure:

$$z = (x_1, y_1, ..., x_n, y_n)^T \tag{10}$$

For the shape formulation, we assume that each trained shape has the same number of related control points n and that the spatial position of each control point i can be modelled with a Gaussian distribution. Figure 5 shows an example of this configuration for a four-shape training set. From this configuration we can obtain some parameters for the family of shapes as the mean shape μ and the covariance Σ of the set.

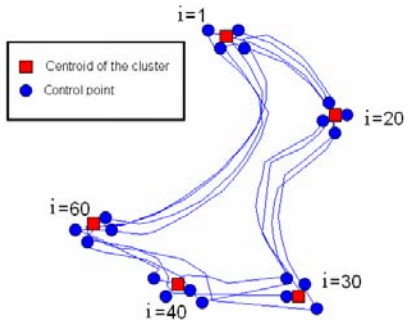

Figure 5: *The figure shows control points i=1,20,30,40,60 of four trained shapes and their related centroids. Each of the shapes is defined by 80 sampled points. The lines in blue show each shape trained after alignment.*

The covariance matrix Σ defines a probability measure for the shape space. If the covariance matrix is full rank, its inverse Σ^{-1} exists and the Gaussian probability distribution of the shape z is :

$$\rho(z) \propto \exp(-\frac{1}{2}(z-\mu)^T \Sigma^{-1}(z-\mu)) \tag{11}$$

Here $\propto$ denotes direct proportionality between the left and

right expressions and μ is the average shape of the training set. The requirement for Σ to be full rank is only accomplished by having at least $2n$ different training shapes. In practical terms, this can be a strong limitation. To solve this problem, a technique of covariance regularization must be applied in order deal with a number of training shapes less than $2n$. We follow the ideas proposed in Cremers et al. [CTWS02] to accomplish this task using $\sigma_\perp = \frac{\sigma_r}{2}$. Finally, it is important to note that the Gaussian probability in equation (11) corresponds to the quadratic energy [CTWS02]:

$$E_c(z) = \log(\rho(z)) + const = -\frac{1}{2}(z-\mu)^T \Sigma_\perp^{-1}(z-\mu) \quad (12)$$

with $const = -log(k)$.

3.2. Incorporating invariance in the shape term

So far, the term E_c in equation (8) is not invariant with respect to similarity transformations of the shape z. For an invariant scheme, the shape of the active contour z is first centered and then aligned with respect to the regularised shapes of the training process. The term representing the centered shape version z_c can be obtained with :

$$z_c = (I_{2n} - \frac{1}{n}\Gamma) \cdot z \quad (13)$$

where I_{2n} denotes the identity matrix of size $2n$, n is the number of control points and the $2n \times 2n$ matrix Γ is given by:

$$\Gamma = \begin{pmatrix} 1 & 0 & 1 & 0 & \dots \\ 0 & 1 & 0 & 1 & \dots \\ 1 & 0 & 1 & 0 & \dots \\ \vdots & \vdots & \vdots & \vdots & \ddots \end{pmatrix} \quad (14)$$

The aligned shape vector $\hat{z}$ is obtained by means of the following expression:

$$\hat{z} = \frac{Mz_c}{|Mz_c|} \quad (15)$$

with:

$$M = I_n \otimes \begin{pmatrix} \mu^T z_c & -\mu^T \times z_c \\ \mu^T \times z_c & \mu^T z_c \end{pmatrix} \quad (16)$$

where I_n is the identity matrix with n rows and the $\otimes$ is the Kroenecker product. For more details of how to obtain these equations see [DM98] and [CTWS02].

4. Results

To test our algorithm, we have designed two groups of experiments: experiments with synthetic images and experiments with real images. The first group uses designed binary images which are synthetic images created with simple geometric objects. This design facilitates comparisons between the expected results and the outcomes of our segmentation approach. For the second category, the experiments were carried out with MR images from the VHP male dataset [Ack98, SASW96]. These MR images were selected from areas of the head with different levels of difficulty in segmenting the skull. The training shape procedure is similar for both groups of experiments and is described in the following subsection.

4.1. Training set creation

In all the experiments, the training set consists of six object shapes, which are in turn made up of a fixed number of sampled points taken along the object's perimeter at equal distances from each other. This number of control points is 40 for synthetic images and 80 for real images.

The trained shapes were acquired with a manual labelling process. The user is presented with an image containing an outline of one object. As the initial step, the user selects with the mouse a number of points on the object contour. The shape of the object is reconstructed from these points by means of a quadratic B-spline interpolation. The resulting curve is resampled and the control points are stored in the same order and number for each shape. This process is repeated six times for each object. For the expermient with synthetic images, the object outlines labelled were one ellipse and one rectangle. For the real images, the training process consists of manually labelling the skull area in the CT image. Even though it seems like a lot of work for the images, the manual segmentation is useful to simulate the variation of the shape distribution. For real images there may be tens or hundreds of images to segment having similar shaped regions, and labelling just six is worthwhile if it gives better results for the rest of the images. Better yet, the results for the rest can then be fed back into the statistical model to improve it.

4.2. Synthetic images

Figure 6 presents the synthetic image designed for the experiment and figure 7 shows some results of our algorithm applied to this image. Each row in figure 7 represents the outcomes of the algorithm for different γ values. The parameter combination is presented in table 1. As expected, setting $\gamma = 0$ results in the whole contour of the composed object being detected (illustrated in the first row). The second row shows a contour 'trapped' between the forces of the GVF potential and the shape potential. In this case, the contour converges to a bad solution with just some portion of the rectangular shape detected. In the third row, the shape term of the snake is high enough to deform the active contour towards the borders of the rectangular contour. Finally, the last two rows show an acceptable approximation to the objects of interest (a rectangle and an ellipse respectively).

4.3. Real images

The next experiment consists of segmenting the bone area shown in figure 2(b). Figure 4 shows its GVF potential cal-

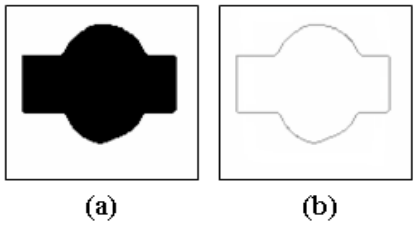

Figure 6: *Synthetic image created with an ellipse and a rectangle overlapped to simulate occlusion (a) The object is represented with a region of zero pixel intensities. (b) The edge map of the image*

Row #	Shape term	Tension Rigidity	Trained shape
1	$\gamma = 0$	$\alpha = \beta = \mu = 0.5$	Rectangle
2	$\gamma = 10$	$\alpha = \beta = \mu = 0.5$	Rectangle
3	$\gamma = 80$	$\alpha = \beta = \mu = 0.5$	Rectangle
4	$\gamma = 100$	$\alpha = \beta = \mu = 0.5$	Rectangle
5	$\gamma = 100$	$\alpha = \beta = \mu = 0.5$	Ellipse

Table 1: *Parameters for segmenting the image in figure 6(b) using a rectangular trained shape.*

culated from a pre-processed thresholded version of this image. Figure 8 displays some results for different γ values. Usually, in the case of a simple active contour after a number of iterations, and depending on the forces directing its evolution, there are two possibilities: it can collapse to a single point or can expand endlessly. In the case of our algorithm, the active contour will always converge to an object silhouette similar in proportions to the trained shape, as illustrated in figure 8(d). In this case the resulting contour is directed by the shape configuration rather than the image features.

As in the case of synthetic images, if the γ value is increased, the shape information influences the outcome, resulting in a scheme directed by the shape. This will compensate for the missing information of bone components of high intensity in the MR image. A very high value of γ will conduct the resulting segmentation to a shape configuration within the distribution of the trained shapes. As can be seen in this figure the result of setting a low shape term gives a poor segmentation of the expected object because of the high variability of pixel intensities in bone regions.

For this region, the average error between the correct segmentation and the final active contour obtained from the MR segmentation is $\bar{e} = 1.97$ pixels (or 0.8mm in real values) with a variance $\sigma^2 = 0.93$ pixels^2 (0.15 mm^2). This error rate is calculated by averaging the distances between the 80 control points from the CT segmentation and the control points from the resulting MR segmentation and assuming that the CT segmentation represents the correct shape at the correct position.

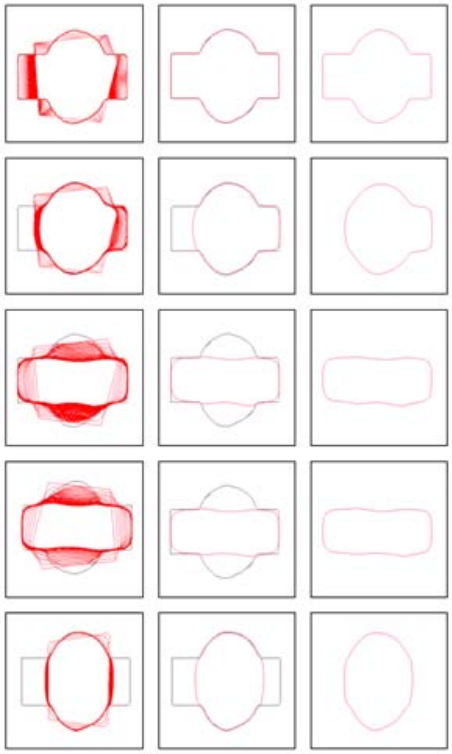

Figure 7: *Extracting one object from the image in figure 6(b). Table 1 gives the parameters used for each row. The first column displays the active contour evolution at each iteration (red lines) overlaid on the feature map (gray pixels). The central column shows a comparison between the final state of the snake and the feature map (gray line). The rightmost column of this figure displays the resulting detected contour.*

Figure 9 shows the result of assembling, by means of a 3D interpolation with Radial Basis Functions [CBC*01], the points of several contours extracted with the algorithm. The image illustrates the results for the upper half of the head for two situations: without shape included and with the shape term included. Figure 10 shows a comparison between the resulting models and a reference CT-segmented model, with the colour-coding based on geometric distance [dS07, RFT04]. In the case of the region presented in figure 10, and for the pure image driven approach (left), the average error is $\bar{e} = 1.46$ mm with $\sigma^2 = 1.25$ mm^2. For the shape included approach (right), the error rate is $\bar{e} = 1.07$ mm with $\sigma^2 = 0.47$ mm^2.

5. Conclusions

We have presented a new, integrated segmentation method that combines an active contour with a shape term, which introduces prior anatomical knowledge to constrain the evo-

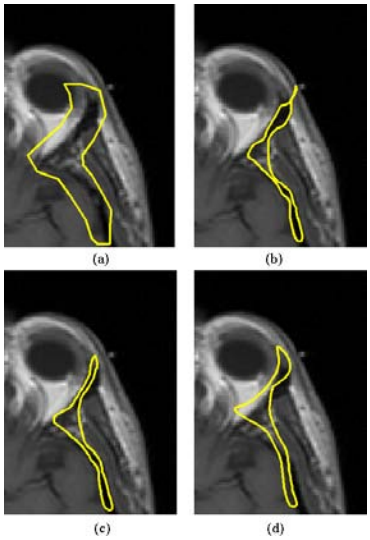

Figure 8: *Results of the MR segmentation for different shape parameters. (a) Initialization. Result for: (b)* $\gamma = 1 \times 10^7$ *(c)* $\gamma = 2 \times 10^7$ *and (d)* $\gamma = 5 \times 10^7$

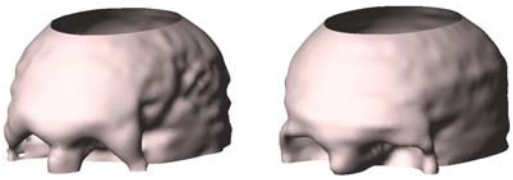

Figure 9: *Results of segmenting the shape without shape term included (left) and with a shape term included (right).*

lution of the snake. The shape term make use of a GVF static potential in contrast to approaches that use a dynamic potential. We have demonstrated the application of the method to the skull segmentation problem for MRI data in a known, difficult to segment region [HHP*97]. Our method has advantages over other approaches in that it can deal with problems such as sub-sampling, occlusion, evolution toward convex areas and incomplete information.

The result of the experiments suggest that if an approximation to the anatomical shape is known, and a good initialisation step is given, then our technique gives acceptable results. In our current work, these two conditions are subject to human intervention. Also, the user currently tunes the parameters to control the shape term in the approach. We are working on automatic techniques to estimate all of these according to the image properties and the spatial location of the object contour to segment. For example, in regular smooth areas of the skull (as in the area above the eye cavities) the shape parameter can be lower than in more complex areas

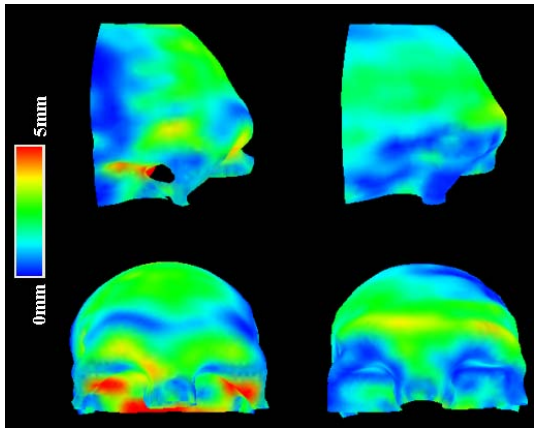

Figure 10: *Colored models representing the geometric distance (mm) between the MR segmented models without (left) and with (right) the shape term included, and a skull model segmented from CT scans. Lateral (top) and frontal(bottom) views of the area around the eye cavities.*

(such as the eye socket region presented as an example in this paper).

The current approach works with 2D contours. We are currently working on a 3D implementation to segment the whole skull as a 3D entity. This 3D implementation will be based on a skull-skin atlas, where the template skull layer will be used to initialise a 3D deformation model by means of a registration process between face layers (since the face layer is easy to extract from MRI data). Statistical knowledge of skull dimensions will also be included in the model to constrain the evolution of the deformable template at each step of the segmentation.

M.S. acknowledges CONACyT-México for the scholarship support, and also thanks Dr. D. Cremers for his valuable comments about diffusion snake implementation.

References

[Ack98] ACKERMAN M.: The Visible Human Project. *Proc. I.E.E.E. 86*, 3 (1998), 504–511.

[AS99] ABRAM F., SANDER P.: Shape Memory for Closed Active Contours. *The 7-th International Conference in Central Europe on Computer Graphics, Visualization and Interactive Digital Media '99* (1999).

[BI98] BLAKE A., ISARD M.: *Active Contours*. Springer, London, 1998.

[CBC*01] CARR J., BEATSON R., CHERRIE J., FRIGHT T. M. W., MCCALLUM B., EVANS T.: Reconstruction and representation of 3D objects with radial basis functions. In *SIGGRAPH* (August 2001), Computer Graphics Proceedings, pp. 67–76.

[CKS97] CASELLES V., KIMMEL R., SAPIRO G.: Geodesic Active Contours. *International Journal of Computer Vision 22*, 1 (1997), 61–79.

[CTWS02] CREMERS D., TSICHHAUSER F., WEICKERT J., SCHNORR C.: Diffusion-Snakes: Introducing Statistical Shape Knowledge into the Mumford-shah functional. In *International Journal of Computer Vision* (2002), vol. 50, pp. 295–313.

[DM98] DRYDEN I., MARDIA K.: *Statistical Shape Analysis*. John Wiley, July 1998.

[dS07] DE SOUSA S.: *PolyMeCo: A Polygonal Mesh Analysis and Comparison Tool*. Master's thesis, Universidad de Aveiro, ETI department, 2007.

[DSL02] DOGDAS B., SHATTUCK D., LEAHY R.: Segmentation of the skull in 3D human MR images using mathematical morphology. In *Proceedings SPIE Medical Imaging Conference* (2002), vol. 4684, pp. 1553–1562.

[Far97] FARIN G.: *Curves and Surfaces for Computer-Aided Geometric Design*. Academic Press, San Diego, 1997.

[FC06] FANG W., CHAN K. L.: Using Statistical Shape Priors in Geodesic Active Contours for Robust Object Detection. *The 18th International Conference on Pattern Recognition* (2006).

[GN94] GUNN S. R., NIXXON M. S.: *A Dual Active Contour Including Parametric Shape*. Tech. Rep. 94, University of Southampton, 1994.

[HF04] HASSAN H., FARAG A. A.: Shape-based MRI data segmentation in the presence of intensity inhomogeneities using level sets. *Elsevier, International Congress Series*, 1268 (2004), 213–218.

[HHP*97] HEINOEN T., H.ESKOLA, P.DASTIDAR, P.LAARNE, J.MALMIVUO: Segmentation of T1 MR scans for reconstruction of resistive head models. *Computer Methods and Programs in Biomedicine 54* (1997), 173–181.

[IT98] INERNEY T. M., TERZOPOULOS D.: Deformable models in medical image analysis: a survey. In *Deformable models in medical image analysis* (1998), Press C. S., (Ed.), IEEE, pp. 2–19.

[KHS03] KÄHLER K., HABER J., SEIDEL H.-P.: Reanimating the Dead: Reconstruction of Expressive Faces from Skull Data. In *ACM Transactions on Graphics* (San Diego, USA, July 2003), of ACM SIGGRAPH 2003 P., (Ed.), pp. 27–31.

[KWT88] KASS M., WITKIN A., TERZOPOULOS D.: Snakes: Active contour methods. *International Journal of Computer Vision* (1988), 312–333.

[LFB98] LADILAW D., FLEISCHER K., BARR A.: Partial-Volume Bayesian Classification of Material Mixtures in MR Volume Data Using Voxel Histograms. *IEEE Transactions on Medical Imaging 17*, 1 (1998), 74–86.

[LMVS03] LEEMPUT K., MAES F., VANDERMEULEN D., SUETENS P.: A Unifying Framework for Partial Volume Segmentation of Brain MR Images. *IEEE Transactions on Medical Imaging 22*, 1 (2003), 105–119.

[PTT02] PITIOT A., TOGA A. W., THOMPSON P. M.: Adaptive Elastic Segmentation of Brain MRI via Shape-Model-Guided Evolutionary Programming. *IEEE Transactions on Medical Imaging 21*, 8 (August 2002), 910–923.

[RBH*99] RIFAI H., BLOCH I., HUTCHINSON S., WIART J., GARNERO L.: Segmentation of the skull in MRI Volumes Using Deformable Model and Taking the Partial Volume Effect into Account. In *SPIE Medical Imaging* (San Diego, California, 1999), vol. 3661, pp. 288–299.

[RFT04] ROY M., FOUFOU S., TRUCHETET F.: Mesh comparison using attribute deviation metric. *International Journal of Image and Graphics 4*, 1 (2004), 1–14.

[SASW96] SPITZER V., ACKERMAN M., SCHERZINGER A., WHITLOCK D.: The Visible Human Male: A Technical Report. *JAMIA 3*, 2 (1996), 118–130.

[SHJ*07] SHAN Z., HUA C., JI Q., PARRA C., YING X., KRASIN M., MERCHANT T., KUN L., REDDICK W.: A Knowledge-guided Active Model of Skull Segmentation on T1-weighted MR images. In *SPIE Medical Imaging* (March 2007), vol. 6512.

[THCB06] TEJOS C., HALL L. D., CARDENAS-BLANCO A.: Segmentation of Articular Cartilage Using Active Contours and Prior Knowlegde. *Proceedings of the 26th Annual International Conference of the IEEE EMBS* (September 2006).

[TWK88] TERZOPOULOS D., WITKIN A., KASS M.: Constraints on deformable models: Recovering 3D shape and nonrigid motion. *Artificial Intelligence 36*, 1 (1988), 91–123.

[VVMN00] VANEZIS P., VANEZIS M., MCCOMBE G., NIBLETT T.: Facial reconstruction using 3-D computer graphics. *Forensic Science International 108*, 2 (February 2000), 81–95.

[Wil04] WILKINSON C.: *Forensic Facial Reconstruction*, 1st ed. Cambridge University Press, United Kingdom, 2004.

[XP96] XU C., PRINCE J. L.: *Snakes, shapes, and gradient vector flow*. Tech. rep., The Johns Hopkins University, October 1996.

[XP97] XU C., PRINCE J. L.: Gradient Vector Flow: A New External Force for Snakes. *IEEE Proceedings Conference on Computer Vision and Pattern Recognition* (1997), 66–71.